Atmos. Chem. Phys. Discuss., 13, 24051–24085, 2013
www.atmos-chem-phys-discuss.net/13/24051/2013/
doi:10.5194/acpd-13-24051-2013

Atmospheric Chemistry and Physics Discussions

Atmospheric parameters in a subtropical cloud regime transition derived by AIRS+MODIS – observed statistical variability compared to ERA-Interim

M. M. Schreier[1,2], B. H. Kahn[2], K. Sušelj[1,2], J. Karlsson[2,3], S. C. Ou[1], Q. Yue[1,2], and S. L. Nasiri[4]

[1]Joint Institute for Regional Earth System Science and Engineering, University of California, Los Angeles, CA, USA
[2]Jet Propulsion Laboratory, California Institute of Technology, Pasadena, CA, USA
[3]Department of Meteorology and Bolin Centre of Climate Research, Stockholm University, Stockholm, Sweden
[4]Department of Atmospheric Sciences, Texas A&M University, College Station, Texas, USA

Received: 18 July 2013 – Accepted: 21 August 2013 – Published: 12 September 2013

Correspondence to: M. M. Schreier (mathias.schreier@jpl.nasa.gov)

Published by Copernicus Publications on behalf of the European Geosciences Union.

Abstract

Cloud occurrence, microphysical and optical properties and atmospheric profiles within a subtropical cloud regime transition in the northeastern Pacific Ocean are obtained from a synergistic combination of the Atmospheric Infrared Sounder (AIRS) and the MODerate resolution Imaging Spectroradiometer (MODIS). The observed cloud parameters and atmospheric thermodynamic profile retrievals are binned by cloud type and analyzed based on their probability density functions (PDFs). Comparison of the PDFs to data from the European Center for Medium Range Weather Forecasting Reanalysis (ERA-Interim) shows a strong difference in the occurrence of the different cloud types compared to clear sky. An increasing non-Gaussian behavior is observed in cloud optical thickness (τ_c), effective radius (r_e) and cloud top temperature (T_c) distributions from Stratocumulus to Trade Cumulus, while decreasing values of lower tropospheric stability are seen. However, variations in the mean, width and shape of the distributions are found. The AIRS potential temperature (θ) and water vapor (q) profiles in the presence of varying marine boundary layer (MBL) cloud types show overall similarities to the ERA-Interim in the mean profiles, but differences arise in the higher moments at some altitudes. The differences between the PDFs from AIRS+MODIS and ERA-Interim make it possible to pinpoint systematic errors in both systems and helps to understand joint PDFs of cloud properties and coincident thermodynamic profiles from satellite observations.

1 Introduction

Earth's cloud types have high variability in both frequency of occurrence and optical properties, and therefore have strong relevance to climate sensitivity (Wyant et al., 2006). This strong variation in cloud types is controlled to a significant degree by the large-scale atmospheric dynamic and thermodynamic structures (Bony and Dufresne, 2005; Su et al., 2008) and its influence in distributions of potential temperature θ and

ACPD
13, 24051–24085, 2013

water vapor q. Quantifying the variations of θ and q within each cloud type is therefore essential for understanding the spatial and temporal variability of clouds in a present and future climate.

Joint probability distribution functions (PDFs) of parameters like potential temperature and total water content can be used to develop subgrid-scale climate model parameterizations to represent variability within a GCM grid (Sommeria and Deardorff, 1977; Cuijpers and Bechthold, 1995). The strong importance of cloud-regime dependent statistics for θ and q is already pointed out by people like Pincus and Klein (2000), Gierens et al. (2007), Pressel and Collins (2013) or Quaas (2012). In particular, Larson et al. (2001) pointed out that global observations of the cloud-type dependence of PDFs in the horizontal, vertical, and temporal domains are necessary for a globally applicable PDF-based parameterization approach.

A particular cloud regime thought to be a significant contributor to uncertainty in the magnitude of climate sensitivity in global climate models is the stratocumulus (Sc) to trade cumulus (trade Cu) transition (Hartmann et al., 1992; Teixeira et al., 2011). It is still a matter of debate which portion of cloudiness within this regime dominates the uncertainty in climate sensitivity (Cess et al., 1989; Wood and Bretherton, 2006; Medeiros et al., 2008). The radiative feedbacks of the various types of marine boundary layer (MBL) clouds show large variations between different GCM simulations (Williams and Webb, 2009). Therefore, detailed observations of cloud properties, thermodynamic profiles, and spectral radiances including their means, variances, and higher order statistical moments are necessary to establish meaningful constraints for climate modeling efforts (Weber et al., 2011).

In situ observations of θ and q profiles over the remote oceans are extremely important sources of information, but they are spatially and temporally limited. For instance, operational radiosonde launches occur regularly but have sparse spatial coverage, whereas field experiments provide well-distributed, but limited time periods (Albrecht et al., 1992; Norris, 1998) and in situ aircraft observations (Price and Wood, 2002; Tompkins, 2003).

ACPD
13, 24051–24085, 2013

Infrared and microwave satellite sounders are capable of continuously observing the global oceans on a daily basis albeit with coarser spatial and temporal resolution, and reduced precision and accuracy, compared to in situ observations. For example, the Atmospheric Infrared Sounder (AIRS)/Advanced Microwave Sounding Unit (AMSU) (Aumann et al., 2003), located on the Earth Observing System (EOS) Aqua satellite, has made these kinds of observations since September 2002. AIRS/AMSU is an advanced sounding suite designed to retrieve temperature and water vapor profiles in clear and cloudy skies for cloud amounts up to and exceeding 70 % (Susskind et al., 2006). The use of infrared retrievals in the lower troposphere remains a challenge due to the decreasing information content in the lower parts of the vertical structure and the difficulty of detecting low cloud contamination. However, recent investigations (e.g., Kahn et al., 2011b; Martins et al., 2011, Yue et al., 2013) show that AIRS/AMSU is capable of observing coarse-layer thermodynamic structures in the planetary boundary layer.

Together with the MODerate resolution Imaging Spectroradiometer (MODIS, Barnes et al., 1998), also located on EOS Aqua, it is possible to observe and estimate clouds with high spatial resolution ($\sim$ 1–5 km, depending on the derived geophysical product) yielding sub-footprint information about cloud variability within the AIRS/AMSU field of view (FOV). Combining the information obtained from the two sensors has resulted in advances in cross-sensor radiance calibration (Tobin et al., 2006; Schreier et al., 2010), synergistic multi-sensor cloud property retrievals (Li et al., 2004a, b) and cloud phase characterization (Kahn et al., 2011a). It is also a useful source of information for radiative transfer calculations under cloudy conditions (Ou et al., 2013) and offers a promising basis for improvements in thermodynamic profile sounding (e.g., Maddy et al., 2011).

The synergistic use of AIRS and MODIS offers a unique opportunity to characterize simultaneous PDFs of θ, q, and cloud properties including optical thickness (τ_c), effective radius (r_e), and cloud top temperature (T_c), and quantify relationships between these variables as a function of cloud type.

ACPD
13, 24051–24085, 2013

In this investigation we explore the combined θ, q, and cloud property PDFs for different oceanic boundary layer cloud types. The Level-2 satellite products are compared to PDFs obtained from the ERA-Interim reanalysis to quantify similarities and differences depending on cloud type. The paper is organized as follows The AIRS thermodynamic soundings and MODIS cloud properties are described in Sect. 2, together with the ERA-Interim data. Section 3 discusses the cloud-type statistical distributions of these properties, including the mean, variance, skewness, and kurtosis of observed cloud parameters and a comparison with ERA-Interim data. Lastly, a discussion, summary and subsequent investigations are presented in Sect. 4.

2 Methodology

2.1 AIRS and MODIS observations

The EOS Aqua platform has a polar sun-synchronous orbit with an equatorial local crossing time of 01:30 (descending) and 13:30 (ascending). AIRS is a grating spectrometer with a spectral resolution of $\nu/\Delta\nu \approx 1200$, a total of 2378 channels in the range of 3.7–15.4 µm with a few spectral gaps, and well-calibrated Level 1B radiances (Overoye, 1999). The AIRS FOV is approximately 1.1°, resulting in a footprint size of 13.5 km at nadir view. There are 90 cross-track scan angles with the highest at ±48.95°, yielding a swath width of approximately 1650 km. AIRS is co-registered with AMSU (Lambrigtsen and Lee, 2003), and the combination is used to retrieve T, q and numerous other surface and atmospheric parameters. Geophysical retrievals are obtained in clear sky and broken cloud cover using a cloud-clearing methodology (Susskind et al., 2003).

The MODIS instrument is a spectrometer based on a spectral filter aperture with 36 channels in the range of 0.4–14 µm and bandwidths of 0.01–0.5 µm, depending on the channel, and scans up to ±55° off nadir view. The pixel size depends on the channel and varies from 0.25–1.0 km at nadir. At 1 km resolution, there are 1354 cross-track

ACPD
13, 24051–24085, 2013

pixels resulting in a swath width of approximately 2330 km. Several MODIS algorithms are designed to obtain a wide variety of land, ocean, and ice surface characteristics, as well as atmospheric and oceanic geophysical properties that include numerous cloud and aerosol parameters. In this work, we use Collection 5 cloud products, including the cloud mask (Ackerman et al., 2008; Frey et al., 2008), effective radius (r_e) and optical thickness (τ_c) (Platnick et al., 2003), and cloud top temperature (T_c) (Menzel et al., 2006).

The MODIS pixels are accurately collocated within the AIRS FOV using the AIRS spatial response functions obtained from prelaunch calibration activities (Schreier et al., 2010). Since AIRS and MODIS have FOV sizes of 1.1° and 0.08° at nadir, respectively, this yields approximately 200 1 km pixels of MODIS within a given AIRS FOV. Using this collocation technique, the importance of each MODIS pixel can be weighted depending on its location within the AIRS spatial response function.

2.2 ERA-Interim reanalysis

The ERA-Interim reanalysis is used as a comparison standard to the satellite observations. The reanalysis is an "interim" following ERA-40 (Uppala et al., 2005), a meteorological reanalysis that uses a wide variety of observations that include synoptic weather information, radiosondes, satellite data, and model forecast data produced by the European Center for Medium-Range Weather Forecasts (ECMWF). The forecast model is the ECMWF Integrated Forecast System (IFS). While satellite data is used in the reanalysis, primarily clear sky AIRS or High Infrared Radiometer Sounder (HIRS) radiances are used; for more details see Dee et al. (2011). The reanalysis spatial resolution is based on a T255 truncation scheme, resulting in ∼ 79 km grid spacing on a reduced Gaussian grid, making it somewhat larger than the AIRS/AMSU footprint at nadir. The timesteps of calculation are 30 min, with an output frequency of 6 h. Cloud top parameters from ERA-Interim were obtained in a manner that mimics the satellite observations. In the case of multi-layer clouds, only the upper layer was considered for T_c and r_e, while liquid water content was vertically integrated over all layers to derive τ_c.

ACPD
13, 24051–24085, 2013

Identical cloud type definitions are applied for satellite observations and ERA-Interim, and they are described in the following section.

2.3 The stratocumulus to trade cumulus transition

Our examination is restricted to the northeastern Pacific Ocean between 0–40° N latitude and 125–175° W longitude. A persistent stratocumulus to trade cumulus transition is bordered by deep convection in the Tropics and mid-latitude baroclinic systems. The highest frequency of stratocumulus occurs from June to September (Klein and Hartmann, 1993). The AIRS and MODIS instruments have provided daily and global data since late 2002. To investigate a reasonable subset of data and minimize inter-annual variations, we focus on all available days in all 7 Julys from 2003–2009 for a total of 217 days.

The emphasis of this study is on the Global Energy and Water Cycle Experiment (GEWEX) Cloud System Study (GCSS) Pacific Cross-Section Inter-comparison (GPCI) transect (Teixeira et al., 2011) using the same area approach described by Karlsson et al. (2010) and is shown in Fig. 1. The track is defined by 12 boxes each with a size of 3° × 4° (latitude × longitude). The centers of the boxes are given by latitude = −1° + (3° × j°) and longitude = 187° + (4° × j°), where $1 \leq j \leq 12$, and j is an integer. The coloring describes the frequency of low cloud coverage for July 2003–2010 according to the International Satellite Cloud Climatology Project (ISCCP) (Rossow and Schiffer, 1999). A snapshot overlay of the MODIS visible 0.65 µm channel is also shown in Fig. 1, highlighting the broken character of MBL clouds in this transitional region. These boxes are chosen as a benchmark for comparisons. The collocation of MODIS and AIRS is performed on the pixel scale within these boxes, with no averaging among the boxes.

The GPCI transect contains a broad range of cloud types. The main three MBL cloud types are namely stratocumulus (Sc), transition cumulus (trans Cu) and trade cumulus (trade Cu). The parameter that differentiates between these three broad MBL cloud categories is the cloud fraction, defined here as the percentage of cloudy pixels within a unit area. There is no precise definition of the spatial scale that applies to cloud

ACPD
13, 24051–24085, 2013

coverage as a discriminant for these three cloud types. To characterize the influence of the cloud type on this study, the MODIS pixel-scale variability within the AIRS FOV was used to determine cloud fraction and the resulting MBL cloud type. In addition to the three categories of MBL cloud types, three additional categories for high clouds, mid-level clouds, and clear sky are included, but no further sub-classification is attempted herein. The definition of each category is based on the MODIS cloud mask *confident cloud* and *probably cloud* categories and cloud top pressure. The flag *probably cloud* was weighted with 50 % cloudy for consistency, but changes in this weighting do not affect the results due to the low frequency of occurrence of this flag in the datasets. The definition of the cloud type within each AIRS FOV is as follows:

- trade Cu: cloud fraction < 30 %, cloud fraction < 1 % for clouds higher than 680 hPa pressure level, latitude < 25° N
- trans Cu: cloud fraction between 30–90 %, cloud fraction < 1 % for clouds higher than 680 hPa pressure level, latitude between 20–30° N
- Sc: cloud fraction > 90 %, cloud fraction < 1 % for clouds higher than 680 hPa pressure level, latitude between 25–35° N
- High clouds (high cld): cloud fraction > 90 % for clouds higher than 440 hPa pressure level, latitude between 0–40° N
- Mid-level clouds (mid cld): cloud fraction > 90 % for clouds between 440–680 hPa, latitude between 0–40° N
- Clear sky (clr): cloud fraction = 0 %, latitude between 0–40° N

Only homogeneous FOVs (cloud fraction > 90 %) are used in the case of mid-level and high clouds to reduce the number of complicated cloud configurations in the study. For clear sky, only the clearest scenes (cloud fraction = 0 %) are retained. Due to the cloud detection limits of MODIS (Ackerman et al., 2008), it is likely that some thin cirrus as

ACPD
13, 24051–24085, 2013

well as subpixel-scale MBL clouds not detected by the MODIS cloud mask are contained in low cloud or clear sky scenes, or that some low clouds were classified as mid-level clouds. However, adjustments in these definitions do not lead to any appreciable changes in the statistics that follow.

The sample sizes exceed 700 000 for AIRS+MODIS and 23 000 for ERA-Interim. However, due to different sampling and retrievals, the cloud and profile statistics are biased towards the specifications of the instruments. Cloud properties were only retained when MODIS retrievals were successful within the AIRS footprint, reducing the total sample size to approximately 500 000 data points. The AIRS/AMSU sounding suite encounters cloud type-dependent sampling rates that may impact the "representativeness" of θ and q statistics within each cloud regime. Only "good" quality profiles are retained; the AIRS "*PGood*" flag must indicate a good retrieval to the ocean surface. Yue et al. (2011) used CloudSat and CALIPSO to quantify the sampling rate by cloud type. AIRS has sampling rates of 80–90 % in areas of trade Cu, and as much as 20–40 % within Sc regimes. In this study, approximately 380 000 profiles with successful retrievals are obtained for the 217-day period. Approximately 48 % of the data are found in trade Cu, 12 % in trans Cu, 7 % in Sc, 16 % in high clouds, 3 % in mid-level clouds, and 14 % in clear sky.

The selection of cloud types and the timeframe of analysis using ERA-Interim were determined in the exact same manner as AIRS/MODIS. The satellite overpasses during daylight are at approximately 13:30 LST (approximately 01:00–04:00 UTC, depending on the location in the cross-section). For consistency, only the 00:00 UTC snapshots from ERA-Interim were used. If the cloud fraction of mid-level or high clouds was below 5 %, the cloud cover in the lower layer was used to determine the presence of clear sky, Sc, trans Cu, or trade Cu. The total sample size is approximately 23 000 with 17% in trade Cu, 36 % in trans Cu, 32 % in Sc, 11 % in high clouds, 1 % in mid-level clouds, and 3 % in clear sky.

ACPD
13, 24051–24085, 2013

2.4 Cloud type statistics of thermodynamic profiles and cloud parameters

AIRS retrievals of θ and q, and MODIS cloud retrievals of r_e, τ_c, and T_c are quantified and sorted by the aforementioned cloud types, and the same procedure is followed for ERA-Interim. To quantify differences between the different cloud types, statistics of each geophysical parameter are calculated separately for each cloud type, and are compared to each other. Given a group of thermodynamic profiles and cloud parameters, the mean, standard deviation, skewness and kurtosis are calculated for each daily "snapshot" and are then averaged for the 217-day period. The second moment (standard deviation) provides information about the variation from the mean. Skewness and kurtosis, the third and fourth moment, provide information about the shape of the distribution function. The skewness helps to identify asymmetry and side-tails, whereas the kurtosis identifies the strength of the "peakedness" of the distribution. In the case of θ and q, the statistics are calculated individually for each vertical layer. This approach was taken to preserve height-dependent behavior in the PDFs. For the cloud parameters, the moments of r_e, τ_c, and T_c are calculated for each cloud type. The interpretations assume a single mode that neglects bimodality, but for the MBL clouds of interest, this assumption is arguably justified. An exception is that bimodality is observed in tropical water vapor (Zhang et al., 2006) and could have an influence on skewness and kurtosis of q, for trade Cu and high clouds.

AIRS and MODIS are not the only instruments of relevance in the A-train for the quantification of the statistical state of MBL clouds in the GPCI cross-section. However, the wide instrument swaths (1600 km and 2330 km, respectively) facilitate the robust calculation of daily instantaneous spatial statistics. The active sensors with a narrow surface track (CloudSat and CALIPSO) do not sample in swaths and thus only the synergy of AIRS and MODIS is emphasized herein.

ACPD
13, 24051–24085, 2013

3 Results

Here we describe the observational and model-derived parameters and their statistical moments. This includes the cloud-type dependent PDFs of r_e, τ_c, and T_c from MODIS, and the Lower Troposheric Stability (LTS), θ, and q from AIRS.

3.1 Cloud parameters

Figure 2 shows the relative occurrence and frequency of cloud fractions of the five defined types of clouds. The occurrence (panel a) for AIRS/MODIS and panel b) for ERA-Interim) is normalized relative to clear sky: 100 % translate as the same occurence of the cloud type as was clear sky occurence for this month, whereas 200 % or 300 % translate as 2 or 3 times more occurence of this type than clear sky. We are using each July month separately and an average over all 7 months (right of black line). ERA-Interim shows over the entire period a much higher occurrence of low marine cloud types than observations. In ERA-Interim, Sc occur on average 18 times more often than clear sky, whereas the observations show a factor of 3.5. Similar differences are seen for trans Cu (ERA-Interim: 20.7, AIRS/MODIS: 1.1) and Sc (ERA-Interim: 7.8, AIRS/MODIS: 1.6). Mid-level clouds (ERA-Interim: 0.8, AIRS/MODIS: 0.7) and high clouds (ERA-Interim: 4.7, AIRS/MODIS: 4.0) are remarkably similar. There is also a substantial variation from year to year with a strong peak in 2005 for ERA-Interim in all cloud types. In the observations, the maximum at 2005 also exists for high clouds, but is reduced for MBL clouds. A detailed investigation of seasonal variations is beyond the scope of this article and will be presented elsewhere.

The PDFs of cloud fraction are shown in the panels c and d of Fig. 2. The frequency of Sc cloud amount is weighted more heavily to near 100 % in MODIS compared to ERA-Interim. For trade Cu and trans Cu, the maximum frequencies are weighted near the bottom (0 %) and top (90 %) of their respective ranges, with a minimum around 30 % cloud fraction. In contrast, ERA-Interim shows a peak frequency of occurrence around 30 % cloud fraction, near the cut-off value for the definition of trade Cu and

ACPD
13, 24051–24085, 2013

trans Cu. Thus, ERA-Interim is producing a higher occurrence frequency of low clouds than observations, but with a lower magnitude of cloud fraction compared to the observations. The limited resolution (250 m to 1 km) of MODIS may result in a shift of trade Cu pixels towards clear sky, but also change the relations of trade Cu in comparison to trans Cu or Sc, which are already overestimated in ERA-Interim. The large differences in occurrence frequency and cloud fraction suggest a biased distribution of cloud liquid water and cloud coverage within ERA-Interim compared to the observations.

Figure 3 shows the statistical distributions of τ_c, T_c, and r_e for each cloud type and is summarized in Table 1. A decrease in the mean τ_c is observed from Sc to trade Cu, consistent with geostationary satellite observations of MBL clouds (Kawai and Teixeira, 2010). The mean values in ERA-Interim are smaller than MODIS, and the decrease from Sc to trade Cu is also much larger in ERA-Interim. Furthermore, the skewness and kurtosis are highest for trade Cu and lowest for Sc in both ERA-Interim and MODIS, also consistent with Kawai and Teixeira (2010). However, ERA-Interim has lower values of skewness and kurtosis compared to MODIS, indicating a more Gaussian behavior (especially for Sc). While MODIS reports a high occurrence of low cloud fraction below 5 % (Fig. 2c) it appears to report much lower occurrences of optically thin trade Cu compared to ERA-Interim (Fig. 2d). These MODIS and ERA-Interim differences in the distribution of liquid water for trade and trans Cu, as seen for occurrence and cloud coverage before, is additionally supported by the differences of optical thickness (Fig. 3a and b).

There are also several notable features in the T_c data (Fig. 3b and e). The mean T_c increases from Sc to trade Cu in both datasets. While T_c increases from 285.1 K in Sc to 295.7 K within trade Cu in MODIS, ERA-Interim only shows an increase from 286.6 to 289.1 K. This is consistent with expectations that trade Cu are found in lower latitudes over warm ocean surfaces compared to Sc. The overestimation of T_c from MODIS is consistent with a warm T_c bias observed in MODIS partly cloudy pixels (Marchand et al., 2010). The large negative skewness observed in T_c, for trade Cu is seen in both MODIS and ERA-Interim and is consistent with a small population of trade Cu skewed

ACPD
13, 24051–24085, 2013

towards higher and colder altitudes capped by a weak trade wind inversion, and a large population at lower and warmer altitudes. In Sc and trans Cu, the distributions of T_c are nearly Gaussian, except for elevated kurtosis of Sc in ERA-Interim.

The mean r_e shows a substantial increase from Sc (12.7 µm) to trade Cu (18.6 µm) in the MODIS data. The ERA-Interim data shows only a weak increase from 11.3 to 12.3 µm. The larger r_e is consistent with the occurrence of larger droplets from stronger updrafts and light precipitation and/or drizzle for r_e larger than 15 µm (Gerber, 1996; Masunaga et al., 2002) and is more realistic than ERA-Interim. For MODIS, the r_e distribution shows a weaker skewness for trade and trans Cu compared to Sc. ERA-Interim has significant non-Gaussian behavior within trade Cu and Sc. The calculation of r_e in ERA-Interim is calculated as a function of height. As a result, the highly non-Gaussian behavior of r_e in ERA-Interim data implies that this simple approach for parameterizing r_e is insufficient for the representation of a realistic PDF of r_e.

The largest variations of T_c that occur within high clouds (σ = 15.2 K for MODIS and 16.6 K for ERA-Interim) is expected because of the wider variety of cloud formations within the less restrictive latitude range (0–40° N). Smaller variations of mid-level clouds are found in MODIS data (σ = 5.6 K), whereas the variations in ERA-Interim are much larger (σ = 14.8). A more detailed inspection of the vertical distribution of clouds reveals that ERA-Interim is distributing the clouds across more height bins between 440–680 hPa compared to MODIS. The largest r_e is found for high clouds (26.9 µm) in the MODIS data, while the mid-level clouds have significantly smaller r_e (12.5 µm) that is very similar to r_e found in Sc. The occurrence of large r_e in high clouds relative to liquid clouds is consistent with extensive in situ and remote sensing observations. In ERA-Interim, the r_e for high (30.0 µm) and mid-level clouds (18.4 µm) is similar to MODIS. However, the distribution functions show that ERA-Interim data is bimodal unlike MODIS.

Overall, the shapes of the PDFs for T_c, τ_c, and r_e are substantially different from each other between the cloud types and between observations and ERA-Interim. Therefore, defining a characteristic PDF shape for all cloud parameters is unjustified and each

ACPD
13, 24051–24085, 2013

parameter should be treated independently as a function of cloud type. Significant differences among the cloud types are observed in the mean values with additional differences in the extent of the PDF tails. The PDFs for MODIS and ERA-Interim show a few remarkable similarities, for instance, similar skewness and kurtosis of the T_c distribution for trade Cu. Some notable differences are the ERA-Interim estimates of r_e, related to an overly simplified approach to calculate r_e compared to MODIS. Differences are also observed for small values of cloud fraction near the limits of MODIS observational capabilities. Thus, the behavior of the PDFs may partly result from retrieval characteristics like assumed constraints on minima and maxima of the cloud parameters, a priori assumptions or other imposed behavior in the cloud retrievals.

3.2 Lower tropospheric stability

The lower tropospheric stability (LTS) is defined as the difference between the potential temperature at 700 hPa and the surface (Klein and Hartmann, 1993) and is proposed as one possibility to constrain cloud fraction in models (Slingo, 1980). Figure 4 shows the distributions of LTS for the three categories of MBL clouds and clear sky from AIRS (panel a) and ERA-Interim (panel b), and Table 2 summarizes the statistical moments. The mean AIRS LTS shows a nearly constant decrease from Sc to trade Cu, consistent with expectations of increasing stability into Sc regions. The ERA-Interim LTS shows somewhat higher mean values, and a bigger jump between trans Cu and Sc than between trade Cu and trans Cu; the reverse is true in AIRS LTS. The mean LTS in clear sky is 3 K higher in AIRS compared to ERA-Interim, and the standard deviation is roughly twice that of the MBL clouds. Recall that clear sky is not restricted in latitude unlike the three MBL cloud types, thus a higher variation in LTS is expected. In the case of ERA-Interim, LTS is smaller than AIRS in clear sky, with smaller standard deviations. The strong positive skewness for trade Cu in both observations and ERA-Interim indicates that the "positive tail" of the trade Cu distribution into high LTS may be realistic. The comparably large skewness and kurtosis for ERA-Interim in the case of clear sky is partly caused by the bi-modal behavior of the distribution and is absent

ACPD
13, 24051–24085, 2013

in MODIS/AIRS. It appears ERA-Interim is often producing clear sky conditions for LTS values where the observations show trade Cu development.

3.3 Temperature profiles

Vertical profiles of θ and q are obtained from the 100-layer AIRS L2 Support product and from ERA-Interim. For the AIRS observations, the examination of the statistical properties of θ and q not only suggest differences related to cloud type, but highlight a few potential, yet subtle, cloud-type dependent retrieval artifacts. The four moments of θ and their day-to-day variability obtained from AIRS and ERA-Interim are shown in Fig. 5. As expected, the mean profiles of θ (panel a and e) are similar for all cloud types in the free troposphere, while more significant differences are found below 850 hPa (panels a and e, insert) and near the tropopause. The inversion is observed for Sc, trans Cu and clear sky around 850–900 hPa in ERA-Interim. In AIRS, rather than observing a sharp inversion, a slight change in lapse rate is seen in the case of Sc and trans Cu. The coarse vertical resolution of AIRS may not be able to resolve vertically shallow weak inversions in the lower troposphere, especially in the presence of Sc, but reasonable results are observed for decreased cloud cover (trans and trade Cu).

The day-to-day variability in AIRS observations is similar to ERA-Interim (indicated by the dotted lines to the left and right of each mean profile), with some differences depending on the particular moment, cloud type and altitude. AIRS θ profiles have a much higher variability in clear sky, when AIRS is expected to have maximum skill, and also for all cloud types compared to ERA-Interim. In the MBL, AIRS has a lower standard deviation of θ (σ_θ) for trans Cu compared to Sc, trade Cu and clear sky. However, ERA-Interim shows similar magnitudes for all MBL clouds, and lower values for clear sky. In general, σ_θ is largest in the MBL and near the tropopause for all cloud types in both AIRS and ERA-Interim. For high clouds, larger values of σ are observed in the MBL and near 250–300 hPa. On average, approximate Gaussian behavior of θ is observed for most of the ERA-Interim profiles that is suggested by low values of skewness and kurtosis and random oscillations along the vertical profile. The exception

ACPD
13, 24051–24085, 2013

is in the MBL, where a slightly higher variability in the higher moments is visible. Similar Gaussian behavior is observed for AIRS data in the case of Sc and trans Cu. Clear sky θ tends to have an increasing positive skewness from the surface to 100 hPa. Trade Cu has a very low skewness in the boundary layer, but shows an increase between 600–700 hPa and again near 200 hPa. An increased kurtosis is observed for clear sky, trade Cu and mid/high clouds for the area between 600–400 hPa. These results demonstrate a systematic change in the distributional characteristics of θ between the MBL and free troposphere in both clear and cloudy sky compared to ERA-Interim. Overall, the observations by AIRS show structured patterns in the profile of the higher moments, whereas the variability is more random in the ERA-Interim data.

AIRS cannot accurately resolve the fine vertical detail of the MBL (Maddy and Barnet, 2008). However a closer examination shows significant differences for the cloud types. First, σ_θ is lower and more uniform for trans Cu than for Sc and trade Cu between 1000 and 850 hPa. Second, skewness and kurtosis for trans Cu and trade Cu near the surface show an increase within the boundary layer and a decrease in the free troposphere. As a modeling benchmark to test these behaviors, Zhu and Zuidema (2009) used field campaign data from eight experiments to simulate MBL structure with a cloud-resolving model. They obtained large vertical variations in the statistics of liquid water potential temperature (θ_l), total water mixing ratio (q_t), and vertical velocity over the depth of the cloud layer. A comparison of Zhu and Zuidema (2009) with AIRS suggests similarities of θ_l and θ in positive skewness of high clouds, but does not reproduce the strong negative skewness seen in Zhu and Zuidema's simulations of trade Cu. AIRS cannot resolve the strong gradients at the top of the broken cloud layers shown in Zhu and Zuidema (2009) and this highlights the importance of obtaining higher vertical resolution thermodynamic soundings than currently available from infrared and microwave satellite sounding.

ACPD
13, 24051–24085, 2013

3.4 Water vapor profiles

The statistical moments of q are summarized in Fig. 6. For AIRS, the mean profile of q is lower for Sc and trans Cu than for trade Cu and clear sky, which is weighted more heavily towards low latitudes because of higher sampling. As expected, the standard deviation of q (σ_q) in panel b is higher in the MBL compared to the free troposphere for all AIRS cloud types. However, σ_q is relatively low for Sc, and is even lower for trans Cu, despite the fact that the mean q is higher than Sc. A subtle but notable feature is a slight increase in σ_q around 800–900 hPa (depending on the MBL cloud type), which coincides with the upper portion of the MBL near the base of the inversion. The ERA-Interim in panel f shows a similar but sharper gradient, which supports the assertion that AIRS is capable of capturing relative differences in the vertical structure of σ_q. With regard to mid-level and high clouds, the largest variations of AIRS σ_q are also observed in the MBL and are much larger than σ_θ. ERA-Interim has a larger gradient of σ_q in the MBL for most cloud types.

The skewness of AIRS snd ERA-Interim (panels c and g) is slightly positive for all cloud types and pressure levels. The AIRS profiles show an increase of this positive skewness within the free troposphere, similar to the kurtosis of θ. This increase is larger for Sc and trans Cu than for clear sky and trade Cu cases indicating that the lower latitudes, where trade Cu and clear sky occur, have stronger positive skewed profiles. ERA-Interim is almost constant throughout the troposphere, with slightly less values in the MBL. The kurtosis of q shows high variations for AIRS observations (panel d). A large increase is observed from Sc to trade Cu at 400 hPa. A qualitative comparison of AIRS q to q_t in Zhu and Zuidema (2009) is partly justified, as water vapor is the dominant part of q_t. An increase in skewness of q_t with altitude is observed in Zhu and Zuidema (2009), consistent with observations of q from AIRS. Furthermore, Iassamen et al. (2009), obtained statistical moments of q from a ground-based microwave profiler over land, dividing measurements into cloudy and clear cases. Similar variations in skewness and kurtosis of q for cloud and clear sky cases in the microwave measure-

ACPD
13, 24051–24085, 2013

ments and AIRS profiles are seen. Overall, the AIRS data, Zhu and Zuidema (2009), and Iassamen (2009) collectively point towards a non-Gaussian cloud type behavior of q not observed in ERA-Interim.

4 Conclusions

A novel pixel-scale application of cloud properties and thermodynamic profiles obtained from the NASA Aqua Moderate Resolution Imaging Spectroradiometer (MODIS) and Atmospheric Infrared Sounder (AIRS) is presented for a subtropical cloud regime transition in the northeastern Pacific Ocean. Simultaneous observations of cloud properties, potential temperature (θ) and water vapor (q) profiles are quantified by cloud type for all available July days from 2003–2009. A co-location method that uses the prelaunch spatial response functions of AIRS is used to obtain robust cloud type estimates within the AIRS field of view using MODIS cloud products. Cloud type dependent estimates of the statistical properties of clouds and thermodynamic profiles are quantified. The focus is within the northeastern Pacific Ocean summertime along the GPCI cross-section, a region well known for a persistent stratocumulus to trade cumulus transition. This marine boundary layer cloud transition is considered to be highly relevant to observational and model assessments of climate sensitivity. Individual AIRS FOVs are sorted into stratocumulus (Sc), transition cumulus (trans Cu), and trade cumulus (trade Cu), mid-level and high clouds, and clear sky. The mean, standard deviation, skewness and kurtosis of the cloud fields and thermodynamic profiles are obtained separately for each cloud type. AIRS and MODIS PDFs are compared to similarly derived PDFs obtained from the ERA-Interim reanalysis.

The analysis of the observed PDFs and their higher moments suggests the following:

– ERA-Interim produces much more MBL clouds, especially trans Cu, than clear sky compared to observations from MODIS.

ACPD
13, 24051–24085, 2013

- Cloud fraction distributions are significantly different for trade Cu, trans Cu and Sc when compared to ERA-Interim.
- The frequency of mid-level and high clouds is overestimated in ERA-Interim compared to observations.
- The distribution of T_c for trade Cu in AIRS+MODIS has higher and more strongly skewed values than ERA-Interim
- A strong skewness in the LTS of trade Cu towards clear sky is seen in observations.
- LTS shows a PDF with strong skewness and bi-modal shape for clear sky cases in the ERA-Interim data, which is not seen in observations.
- In the free troposphere, clear sky and trade Cu both exhibit significant non-Gaussian behavior near 700 and 400 hPa for observations, which is not seen in ERA-Interim
- For both θ and q, lower standard deviations are observed in the MBL in ERA-Interim and observations.
- A positive kurtosis of q in the free troposphere is seen for observations but not for ERA-Interim.
- ERA-Interim and observations have a similar vertical structure, but a reduced magnitude in the standard deviation of ERA-Interim is noted.
- ERA-Interim shows reduced magnitudes in skewness and kurtosis, indicating a more Gaussian behavior than observations.

Knowing the distributional characteristics of cloud and thermodynamic properties for different types of clouds is necessary for implementing a subgrid-scale parameterization of cloud processes in climate models. The results obtained from the synergistic,

ACPD
13, 24051–24085, 2013

pixel-scale MODIS and AIRS observations offer important constraints on the spatial, temporal, and cloud type variability in these PDFs.

Future work will include tests for the cloud reproduction an extension of this method to other MBL transitional regimes, and an expansion to other cloud regimes throughout the seasonal cycles.

Acknowledgements. Funding for this project was provided by NASA award NNX08AI09G. The authors would like to thank João Teixeira and the AIRS project at the Jet Propulsion Laboratory for encouragement and support. MODIS data were obtained through the Level-1 and Atmosphere Archive and Distribution System (LAADS; http://ladsweb.nascom.nasa.gov/). AIRS data were obtained through the Goddard Earth Sciences Data and Information Services Center (http://daac.gsfc.nasa.gov). A portion of this work was performed within the Joint Institute for Regional Earth System Science & Engineering (JIFRESSE) of the University of California, Los Angeles (UCLA) and at the Jet Propulsion Laboratory, California Institute of Technology, under contract with NASA.

References

Ackerman, S. A., Holz, R. E., Frey, R., Eloranta, E. W., Maddux, B. C., and McGill, M.: Cloud detection with MODIS. Part II: Validation, J. Atmos. Ocean. Tech., 25, 1073–1086, 2008.

Albrecht, B. A., Bretherton, C. S., Johnson, D., Scubert, W. H., and Frisch, A. S.: The Atlantic Stratocumulus Transition Experiment – ASTEX, B. Am. Meteorol. Soc., 76, 889–904, 1995.

Aumann, H. H., Chahine, M. T., Gautier, C., Goldberg, M., Kalnay, E., McMillin, L., Revercomb, H., Rosenkranz, P. W., Smith, W. L., Staelin, D., Strow, L., and Susskind, J.: AIRS/AMSU/HSB on the aqua mission: Design, science objectives, data products, and processing systems, IEEE T. Geosci. Remote Sens., 41, 253–264, 2003.

Barnes, W. L., Pagano, T. S., and Salomonson, V. V.: Prelaunch characteristics of the Moderate Resolution Imaging Spectroradiometer (MODIS) on EOS-AM1, IEEE T. Geosci. Remote Sens., 36, 1088–1100, 1998.

ACPD

13, 24051–24085, 2013

Bony, S. and Dufresne, J.-L.: Marine boundary layer clouds at the heart of tropical cloud feedback uncertainties in climate models, Geophys. Res. Lett., 32, L20806, doi:10.1029/2005GL023851, 2005.

Cess, R., Potter, G. L., Blanchet, J. P., Boer, G. J., Ghan, S. J., Kiehl, J. T., Treut, H. L., Li, Z.-X., Liang, X.-Z., Mitchell, J. F. B., Morcrette, J.-J., Randall, D. A., Riches, M., Roeckner, E., Schlesse, U., Slingo, A., Taylor, E. E., Washington, W. M., Wetherald, R. T., and Yagai, I.: Interpretation of cloud-climate feedback as produced by 14 atmospheric general circulation models, Science, 245, 513–516, 1989.

Chen, T., Rossow, W. B., and Zhang, Y.: Radiative effects of cloud-type variations, J. Climate, 13, 264–286, 2000.

Cuijpers, J. W. M. and Bechtold, P.: A simple parameterization of cloud water related variables for use in boundary layer models, J. Atmos. Sci., 52, 2486–2490, 1995.

Dee, D. P., Uppala, S. M., Simmons, A. J., Berrisford, P., Poli, P., Kobayashi, S., Andrae, U., Balmaseda, M. A., Balsamo, G., Bauer, P., Bechtold, P., Beljaars, A. C. M., van de Berg, L., Bidlot, J., Bormann, N., Delsol, C., Dragani, R., Fuentes, M., Geer, A. J., Haimberger, L., Healy, S. B., Hersbach, H., Hólm, E. V., Isaksen, L., Kållberg, P., Köhler, M., Matricardi, M., McNally, A. P., Monge-Sanz, B. M., Morcrette, J.-J., Park, B.-K., Peubey, C., de Rosnay, P., Tavolato, C., Thépaut, J.-N., and Vitart, F.: The ERA-Interim reanalysis: configuration and performance of the data assimilation system, Q. J. Roy. Meteor. Soc., 137, 553–597, doi:10.1002/qj.828, 2011.

Fetzer, E. J., Teixeira, J., Olsen, E. T., and Fishbein, E. F.: Satellite remote sounding of atmospheric boundary layer temperature inversions over the subtropical eastern Pacific, Geophys. Res. Lett., 31, L17102, doi:10.1029/2004GL020174, 2004.

Frey, R. A., Ackerman, S. A., Liu, Y., Strabala, K. I., Zhang, H., Key, J. R., and Wang, X.: Cloud detection with MODIS. Part I: Improvements in the MODIS cloud mask for Collection 5, J. Atmos. Ocean. Tech., 25, 1057–1072, 2008.

Gerber, H.: Microphysics of marine stratocumulus clouds with two drizzle modes, J. Atmos. Sci., 53, 1649–1662, 1996.

Gierens, K., Kohlhepp, R., Dotzek, N., and Smit, H. G.: Instantaneous fluctuations of temperature and moisture in the upper troposphere and tropopause region. Part 1: Probability densities and their variability, Meteor. Z., 16, 221–231, 2007.

Hartmann, D., Ockert-Bell, M., and Michelsen, M.: The effect of cloud type on Earth's energy balance: Global analysis, J. Climate, 5, 1281–1304, 1992.

ACPD
13, 24051–24085, 2013

Iassamen, A., Sauvageot, H., Jeannin, N., and Ameur, S.: Distribution of tropospheric water vapor in clear and cloudy conditions from microwave radiometric profiling, J. Appl. Meteor. Climatol., 48, 600–615, 2009.
Kahn, B. H., Nasiri, S. L., Schreier, M. M., and Baum, B. A.: Impacts of sub-pixel cloud heterogeneity on infrared thermodynamic phase assessment, J. Geophys. Res., 116, D20201, doi:10.1029/2011JD015774, 2011a.
Kahn, B. H., Teixeira, J., Fetzer, E. J., Gettelman, A., Hristova-Veleva, S. M., Huang, X., Kochanski, A. K., Kohler, M., Krueger, S. K., Wood, R., and Zhao, M.: Temperature and Water Vapor Variance Scaling in Global Models: Comparisons to Satellite and Aircraft Data, J. Atmos. Sci., 68, 2156–2168, doi:10.1175/2011JAS3737.1, 2011b.
Karlsson, J., Svensson, G., Cardoso, S., Teixeira, J., and Paradise, S.: Subtropical Cloud-Regime Transitions: Boundary Layer Depth and Cloud-Top Height Evolution in Models and Observations, J. Appl. Meteor. Climatol., 49, 1845–1858, 2010.
Kawai, H. and Teixeira, J.: Probability density functions of liquid water path and cloud amount of marine boundary layer clouds: Geographical and seasonal variations and controlling meteorological factors, J. Climate, 23, 2079–2092, 2010.
Klein, S. A. and Hartmann, D. L. The seasonal cycle of low stratiform clouds, J. Climate, 6, 1587–1606, 1993.
Lambrigtsen, B. H. and Lee, S.-Y.: Coalignment and synchronization of the AIRS instrument suite, IEEE T. Geosci. Remote Sens., 41, 343–351, 2003.
Larson, V. E., Wood, R., Field, P. R., Golaz, J.-C., Vonder Haar, T. H., and Cotton, W. R.: Small-Scale and mesoscale variability of scalars in cloudy boundary layers: One-dimensional probability density functions, J. Atmos. Sci., 58, 1978–1994, 2001.
Li, J., Menzel, W. P., Sun, F., Schmit, T. J., and Gurka, J.: AIRS subpixel cloud characterization using MODIS cloud products, J. Appl. Meteorol., 43, 1083–1094, 2004a.
Li, J., Menzel, W. P., Zhang, W., Sun, F., Schmit, T. J., Gurka, J. J., and Weisz, E.: Synergistic use of MODIS and AIRS in a variational retrieval of cloud parameters, J. Appl. Meteorol., 43, 1619–1634, 2004b.
Maddy, E. S. and Barnet, C. D.: Vertical resolution estimates in version 5 of AIRS operational retrievals, IEEE T. Geosci. Remote Sens., 46, 2375–2384, 2008.
Maddy, E. S., King, T. S., Sun, H., Wolf, W. W., Barnet, C. D., Heidinger, A., Cheng, Z., Goldberg, M. D., Gambacorta, A., Zhang, C., and Zhang, K.: Using Metop-A AVHRR clear-sky

ACPD
13, 24051–24085, 2013

measurements to cloud-clear Metop-A ISAI column radiances, J. Atmos. Ocean. Tech., 28, 1104–1116, doi:10.1175/JTECH-D-10-05045.1, 2011.
Marchand, R., Ackerman, T., Smyth, M., and Rossow, W. B.: A review of cloud top height and optical depth histograms from MISR, ISCCP, and MODIS, J. Geophys. Res., 115, D16206, doi:10.1029/2009JD013422, 2010.
Martins, J. P. A., Teixeira, J., Soares, P. M. M., Miranda, P. M. A., Kahn, B. H., Dang, V. T., Irion, F. W., Fetzer, E. J., and Fishbein, E.: Infrared sounding of the trade-wind boundary layer: AIRS and the RICO experiment, Geophys. Res. Lett., 37, L24806, doi:10.1029/2010GL045902, 2011.
Masunaga, H., Nakajima, T. Y., Nakajima, T., Kachi, M., and Suzuki, K.: Physical properties of maritime low clouds as retrieved by combined use of Tropical Rainfall Measuring Mission (TRMM) Microwave Imager and Visible/Infrared Scanner, 2. Climatology of warm clouds and rain, J. Geophys. Res., 107, 4367, doi:10.1029/2001JD001269, 2002.
Medeiros, B., Stevens, B., Held, I. M., Zhao, M., Williamson, D. L., Olson, J. G., and Bretherton, C. S.: Aquaplanets, climate sensitivity, and low clouds, J. Climate, 21, 4974–4991, 2008.
Menzel, W. P., Baum, B. A., Strabala, K. I., and Frey, R. A.: Cloud top properties and cloud phase, MODIS Algorithm Theoretical Basis Document, NASA, 2006.
Nasiri, S. L., Dang, H. V. T., Kahn, B. H., Fetzer, E. J., Manning, E. M., Schreier, M. M., and Frey, R. A.: Comparing MODIS and AIRS infrared-based cloud retrievals, J. Appl. Meteorol. Clim., 50, 1057–1072, 2011.
Norris, J. R.: Low cloud type over the ocean from surface observations. Part I: relationship to surface meteorology and the vertical distribution of temperature and moisture, J. Climate, 11, 369–382, 1998.
Ou, S.-C., Kahn, B. H., Liou, K. N., Takano, Y., Schreier, M. M., and Yue, Q.: Retrieval of cirrus cloud properties from the Atmospheric Infrared Sounder: The k-coefficient approach combined with SARTA plus delta-four stream approximation, IEEE T. Geosci. Remote Sens., 51, 1010–1024, 2013.
Overoye, K., Aumann, H. H., Weiler, M. H., Gigioli, G. W., Shaw, W., Frost, E., and McKay, T.: Test and Calibration of the AIRS instrument, SPIE Proceedings, 3759, 254–265, 1999.
Pincus, R. and Klein, S. A.: Unresolved spatial variability and microphysical process rates in large-scale models, J. Geophys. Res., 105, 27059–27065, 2000.

ACPD
13, 24051–24085, 2013

Platnick, S., King, M. D., Ackerman, S. A., Menzel, W. P., Baum, B. A., Riédi, J. C., and Frey, R. A.: The MODIS cloud products: Algorithms and examples from Terra, IEEE T. Geosci. Remote Sens., 41, 459–473, 2003.

Pressel, K. G. and Collins, W. D.: First order structure function analysis of statistical scale invariance in the observed AIRS water vapor field, J. Climate, 25, 5538–5555, 2013.

Price, J. D. and Wood, R.: Comparison of probability density functions for total specific humidity and saturation deficit humidity, and consequences for cloud parameterization, Q. J. Roy. Meteor. Soc., 128, 2059–2072, 2002.

Quaas, J.: Evaluating the "critical relative humidity" as a measure of subgrid-scale variability of humidity in general circulation model cloud cover parameterizations using satellite data, J. Geophys. Res., 117, D09208, doi:10.1029/2012JD017495, 2012.

Ramanathan, V., Cess, R. D., Harrison, E. F., Minnis, P., Barkstrom, B. R., Ahmad, E., and Hartmann, D.: Cloud-radiative forcing and climate: Results from the Earth Radiation Budget Experiment, Science, 243, 57–63, 1989.

Rossow, W. B. and Schiffer, R. A.: Advances in Understanding Clouds from ISCCP, B. Am. Meteorol. Soc., 72, 2–20, 1999.

Schreier, M. M., Kahn, B. H., Eldering, A., Elliott, D. A., Fishbein, E., Irion, F. W., and Pagano, T. S.: Radiance comparisons of MODIS and AIRS using spatial response information, J. Atmos. Ocean. Tech., 27, 1331–1342, 2010.

Slingo, J. M.: A cloud parametrization scheme derived from GATE data for use with a numerical model, Q. J. Roy. Meteor. Soc., 106, 747–770, doi:10.1002/qj.49710645008, 1980.

Solomon, S., Qin, D., Manning, M., Marquis, M., Averyt, K., Tignor, M. M. B., Miller Jr., H. L., and Chen, Z.: Climate Change 2007: The Physical Science Basis, Cambridge, University Press, 996 pp., 2007.

Sommeria, G. and Deardorff, J. W.: Subgrid-scale condensation in models of nonprecipitating clouds, J. Atmos. Sci., 34, 344–355, 1977.

Stephens, G. L.: Cloud feedbacks in the climate system: A critical review, J. Climate, 18, 237–273, 2005.

Su, H., Jiang, J. H., Vane, D. G., and Stephens, G. L.: Observed vertical structure of tropical oceanic clouds sorted in large-scale regimes, Geophys. Res. Lett., 35, L24704, doi:10.1029/2008GL035888, 2008.

ACPD
13, 24051–24085, 2013

Susskind, J., Barnet, C. D., and Blaisdell, J. M.: Retrieval of atmospheric and surface parameters from AIRS/AMSU/HSB data in the presence of clouds, IEEE T. Geosci. Remote Sens., 41, 390–409, 2003.

Susskind, J., Barnet, C., Blaisdell, J., Iredell, L., Keita, F., Kouvaris, L., Molnar, G., and Chahine, M.: Accuracy of geophysical parameters derived from Atmospheric Infrared Sounder/Advanced Microwave Sounding Unit as a function of fractional cloud cover, J. Geophys. Res., 111, D09S17, doi:10.1029/2005JD006272, 2006.

Teixeira, J., Cardoso, S., Bonazzola, M., Cole, J., DelGenio, A., DeMott, C., Franklin, C., Hannay, C., Jakob, C., Jiao, Y., Karlsson, J., Kitagawa, H., Koehler, M., Kuwano-Yoshida, A., Ledrian, C., Lock, A., Miller, M. J., Marquet, P., Martins, J., Mechoso, C. R., Meijgaard, E. V., Meinke, I., Miranda, P. M. A., Mironov, D., Neggers, R., Pan, H. L., Randall, D. A., Rasch, P. J., Rockel, B., Rossow, W. B., Ritter, B., Siebesma, A. P., Soares, P., Turk, F. J., Vaillancourt, P., Von Engeln, A., and Zhao, M.: Tropical and subtropical cloud transitions in weather and climate prediction models: the GCSS/WGNE Pacific Cross-section Inter-comparison (GPCI), J. Climate, 24, 5223–5256, doi:10.1175/2011JCLI3672.1, 2011.

Tobin, D. C., Revercomb, H. E., Moeller, C. C., and Pagano, T. S.: Use of AIRS high spectral resolution spectra to assess the calibration of MODIS on EOS Aqua, J. Geophys. Res., 111, D09S05, doi:10.1029/2005JD006095, 2006a.

Tompkins, A. M.: Impact of temperature and humidity variability on cloud cover assessed using aircraft data, Q. J. Roy. Meteor. Soc., 129, 2151–2170, doi:10.1256/qj.02.190, 2003.

Uppala, S. M., KÅllberg, P. W., Simmons, A. J., Andrae, U., Bechtold, V. D. C., Fiorino, M., Gibson, J. K., Haseler, J., Hernandez, A., Kelly, G. A., Li, X., Onogi, K., Saarinen, S., Sokka, N., Allan, R. P., Andersson, E., Arpe, K., Balmaseda, M. A., Beljaars, A. C. M., Berg, L. V. D., Bidlot, J., Bormann, N., Caires, S., Chevallier, F., Dethof, A., Dragosavac, M., Fisher, M., Fuentes, M., Hagemann, S., Hólm, E., Hoskins, B. J., Isaksen, L., Janssen, P. A. E. M., Jenne, R., Mcnally, A. P., Mahfouf, J.-F., Morcrette, J.-J., Rayner, N. A., Saunders, R. W., Simon, P., Sterl, A., Trenberth, K. E., Untch, A., Vasiljevic, D., Viterbo, P., and Woollen, J.: The ERA-40 re-analysis, Q. J. Roy. Meteor. Soc., 131, 2961–3012, doi:10.1256/qj.04.176, 2005.

Weber, T., Quaas, J., and Räisänen, R.: Evaluation of the statistical cloud scheme in the ECHAM5 model using satellite data, Q. J. Roy. Meteor. Soc., 137, 2079–2091, 2011.

Weisz, E., Menzel, W. P., Smith, N., Frey, R., Borbas, E. E., and Baum, B. A.: An Approach for Improving Cirrus Cloud Top Pressure/Height Estimation by Merging High Spatial Resolution

ACPD
13, 24051–24085, 2013

Infrared Window Imager Data with High Spectral Resolution Sounder Data, J. Appl. Meteorol. Clim., 51, 1477–1488, doi:10.1175/JAMC-D-11-0170.1, 2012.
Williams, K. D. and Webb, M. J.: A quantitative performance assessment of cloud regimes in climate models, Clim. Dynam., 33, 141–157, doi:10.1007/s00382-008-0443-1, 2009.
Wood, R. and Bretherton, C. S.: On the relationship between stratiform low cloud cover and lower-tropospheric stability, J. Climate, 19, 6425–6432, 2006.
Wyant, M. C., Bretherton, C. S., Bacmeister, J. T., Kiehl, J. T., Held, I. M., Zhao, M., Klein, S. A., and Soden, B. J.: A comparison of low-latitude cloud properties and their response to climate change in three AGCMs sorted into regimes using mid-tropospheric vertical velocity, Clim. Dynam., 27, 261–279, doi:10.1007/s00382-006-0138-4, 2006.
Yue, Q., Kahn, B. H., Fetzer, E. J., and Teixeira, J.: Relationship between oceanic boundary layer clouds and lower tropospheric stability observed by AIRS, CloudSat, and CALIOP, J. Geophys. Res., 116, D18212, doi:10.1029/2011JD016136, 2011.
Yue, Q., Fetzer, E., Kahn, B., Wong, S., Manipon, G., Guillaume, A., and Wilson, B.: Cloud-state-dependent Sampling in AIRS Observations based on CloudSat Cloud Classification, J. Climate, doi:10.1175/JCLI-D-13-00065.1, in press, 2013.
Zhang, C., Mapes, B. E., and Soden, B. J.: Bimodality in tropical water vapor, Q. J. Roy Meteor. Soc., 129, 2847–2866, 2006.
Zhu, P. and Zuidema, P.: On the use of PDF schemes to parameterize sub-grid clouds, Geophys. Res. Lett., 36, L05807, doi:10.1029/2008GL036817, 2009.

ACPD
13, 24051–24085, 2013

Table 1. Mean, standard deviation, skewness and kurtosis of MODIS derived ("S" for satellite columns) and ERA-Interim derived ("M" for model columns) cloud parameters (τ_c, r_e, T_c) for five different cloud types (defined in Sect. 2).

Cloud optical thickness	Mean		Stddev		Skewness		Kurtosis	
	S	M	S	M	S	M	S	M
Trade cu	4.2	0.8	3.7	0.5	2.1	1.2	6.7	2.1
Transition cloud	4.9	2.3	2.9	1.1	1.5	1.0	3.7	1.4
Stratocumulus	8.9	5.4	4.8	1.9	1.4	0.4	3.1	0.1
High clouds	9.2	2.2	9.9	3.4	1.8	3.2	3.2	11.5
Mid-level clouds	12.2	8.9	5.9	6.2	1.4	1.4	3.5	2.9
Effective radius (μm)	Mean		Stddev		Skewness		Kurtosis	
	S	M	S	M	S	M	S	M
Trade cu	18.6	12.3	5.6	0.8	0.2	11.0	0.5	222.3
Transition cloud	17.1	12.1	5.7	0.4	0.1	−0.2	−1.0	−0.1
Stratocumulus	12.7	11.3	4.4	0.5	1.0	3.7	0.3	41.5
High clouds	26.9	30.0	6.6	3.9	0.3	−0.4	0.6	−1.1
Mid-level clouds	12.5	18.4	5.0	3.8	1.5	1.2	1.6	1.6
Cloud top temp (K)	Mean		Stddev		Skewness		Kurtosis	
	S	M	S	M	S	M	S	M
Trade cu	295.7	289.1	3.5	2.9	−6.8	−12.4	122.8	270.9
Transition cloud	290.0	287.8	2.2	1.5	−0.2	−0.4	0.3	0.7
Stratocumulus	285.1	286.6	2.1	1.6	0.2	−1.2	−0.3	12.5
High clouds	222.4	222.2	15.2	16.6	0.4	1.9	−0.6	5.0

ACPD
13, 24051–24085, 2013

Table 2. Mean, standard deviation, skewness and kurtosis of AIRS-derived lower tropospheric stability (LTS) for three marine boundary layer (MBL) cloud types and clear sky (defined in Sect. 2).

Lower trop. stability (K)	Mean		Stddev		Skewness		Kurtosis	
	S	M	S	M	S	M	S	M
Trade cu	16.6	20.3	2.5	1.7	0.6	0.6	0.2	0.1
Transition cloud	21.1	22.3	2.3	2.2	0.3	0.5	0.3	0.0
Stratocumulus	24.5	26.4	3.2	2.8	0.3	−0.1	0.0	−0.1
Clear Sky	25.1	22.2	7.1	3.0	−0.1	0.4	−1.3	−0.5

ACPD
13, 24051–24085, 2013

Table 3. Acronyms and symbols used in text.

q	water vapor mixing ratio
q_t	total water mixing ratio
θ	potential temperature
θ_l	liquid potential temperature
T_c	cloud top temperature
r_e	cloud effective radius
τ_c	cloud optical thickness
LTS	lower tropospheric stability
σ_q	standard deviation of water vapor mixing ratio
σ_θ	standard deviation of potential temperature

ACPD
13, 24051–24085, 2013

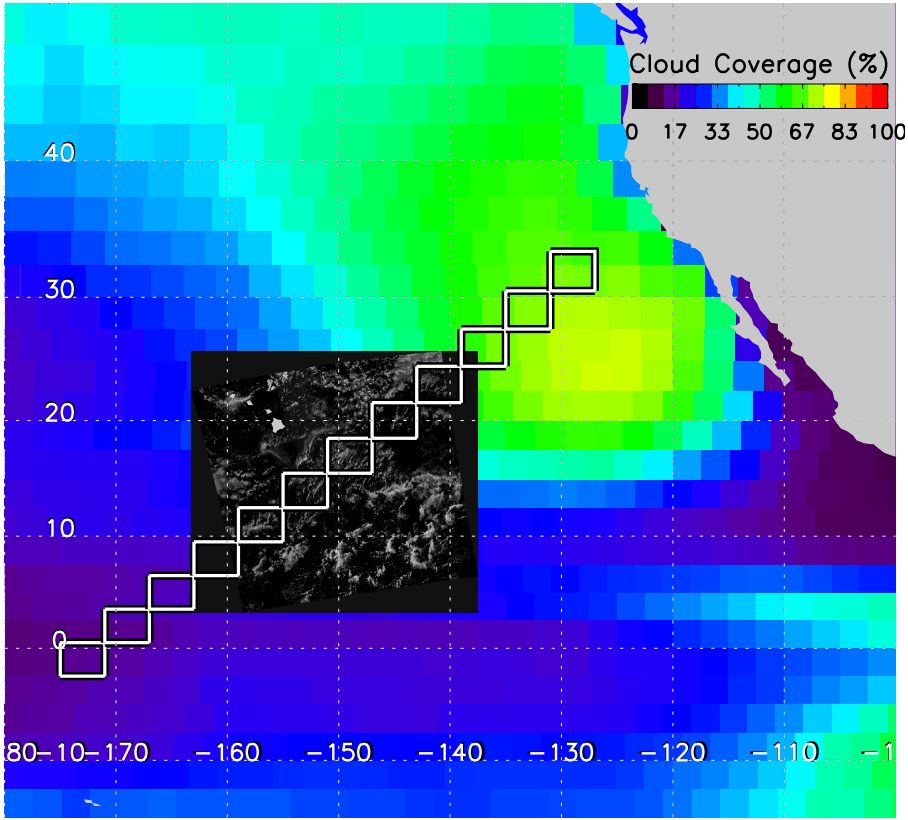

Fig. 1. Shown is the primary region of interest in the northeastern Pacific Ocean along the GPCI transect (white boxes; Karlsson et al., 2010; Teixeira et al., 2011). The colored background is the mean low cloud amount according to ISCCP (Rossow and Schiffer, 1999) for a July composite from 2003–2010. The overlay is a snapshot image from the 0.65 µm channel of MODIS from 1 July 2007.

ACPD
13, 24051–24085, 2013

Atmospheric parameters in a subtropical cloud regime transition

M. M. Schreier et al.

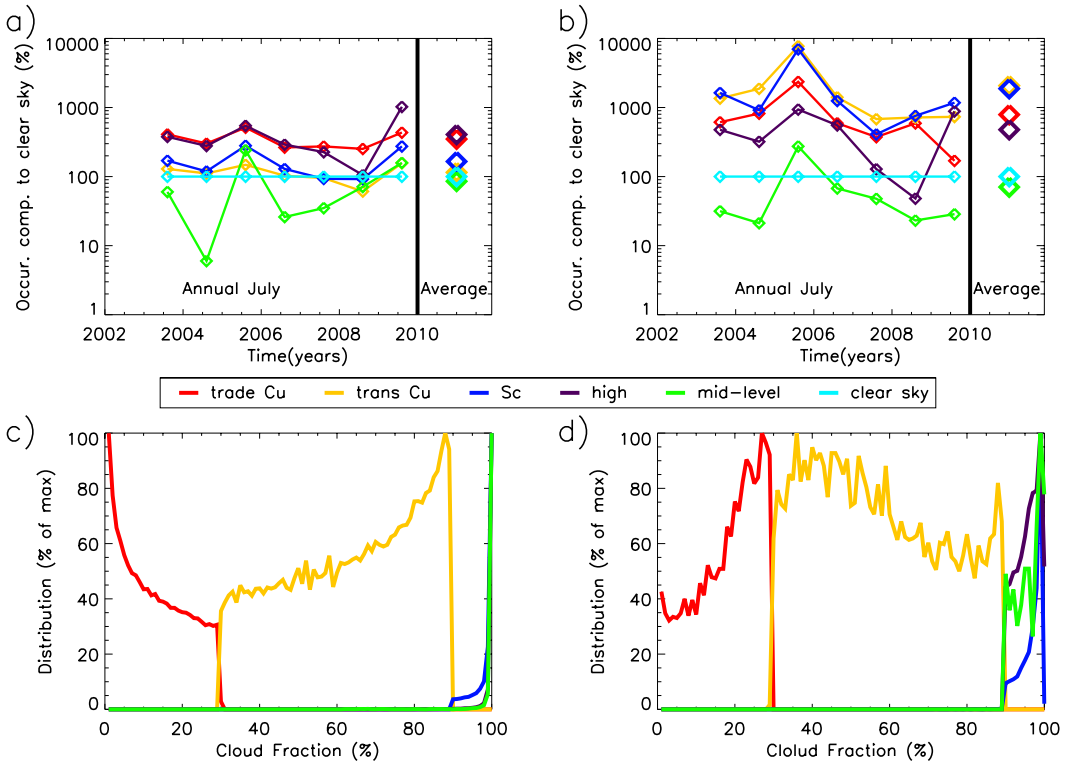

Fig. 2. Annual and average occurrence of cloud types relative to clear sky (panels **a** and **b**) and cloud fraction (panels **c** and **d**) for the entire 217-day data set. The left column is for the AIRS/MODIS observations, and the right is for ERA-Interim.

ACPD
13, 24051–24085, 2013

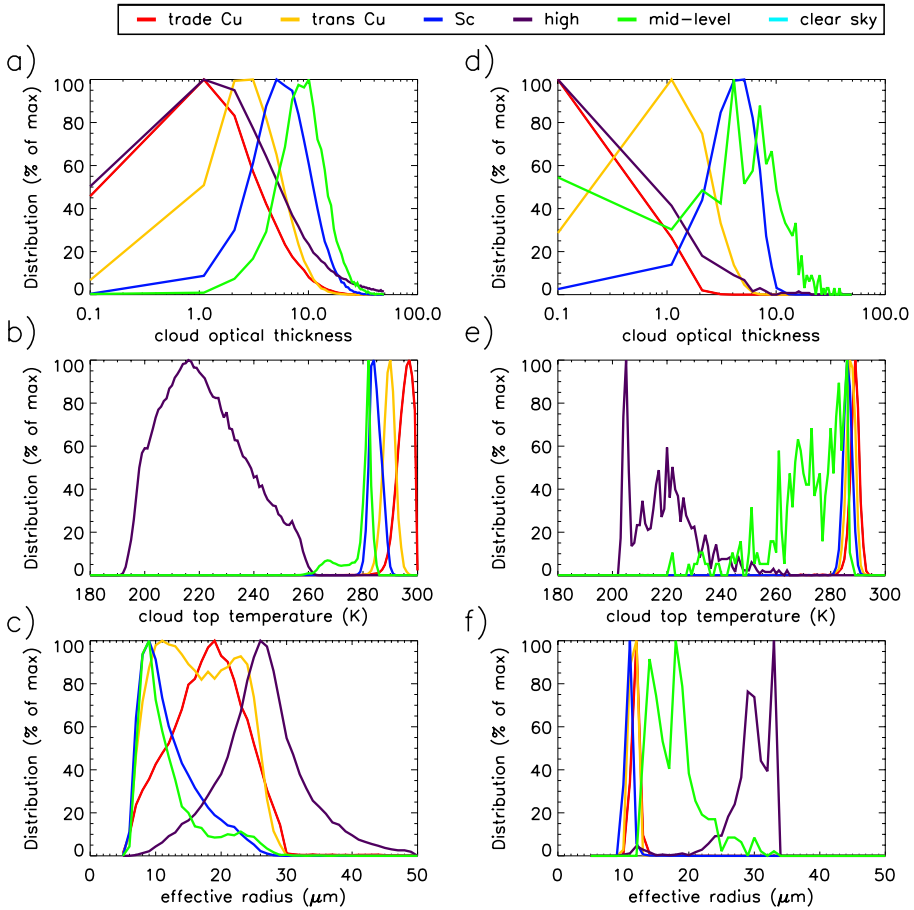

Fig. 3. Cloud-type distributions of τ_c (panels **a** and **d**), T_c (panels **b** and **e**), r_e (panels **c** and **f**) for the entire 217-day data set. The left column is for the AIRS/MODIS observations, and the right is for ERA-Interim.

ACPD
13, 24051–24085, 2013

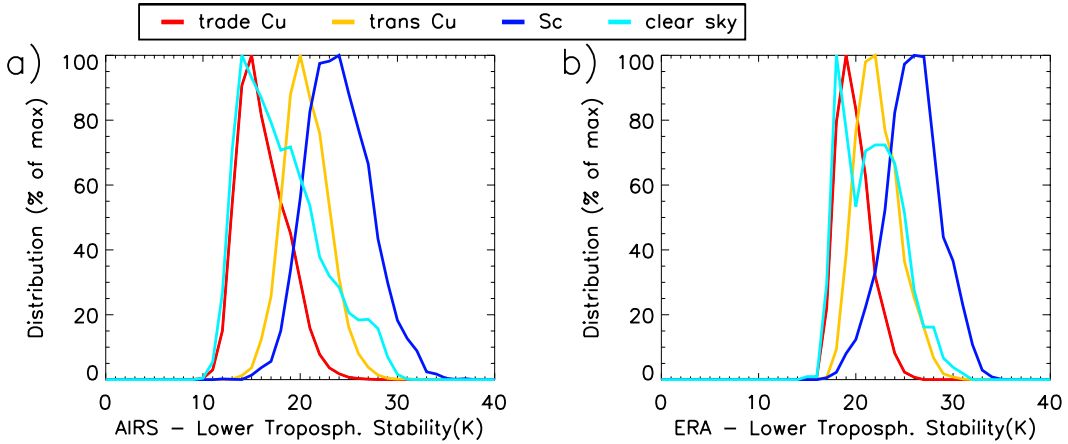

Fig. 4. Cloud-type distributions of lower tropospheric stability for the entire 217-day data set. Panel **(a)** is for the AIRS/MODIS observations, and panel **(b)** for ERA-Interim.

ACPD
13, 24051–24085, 2013

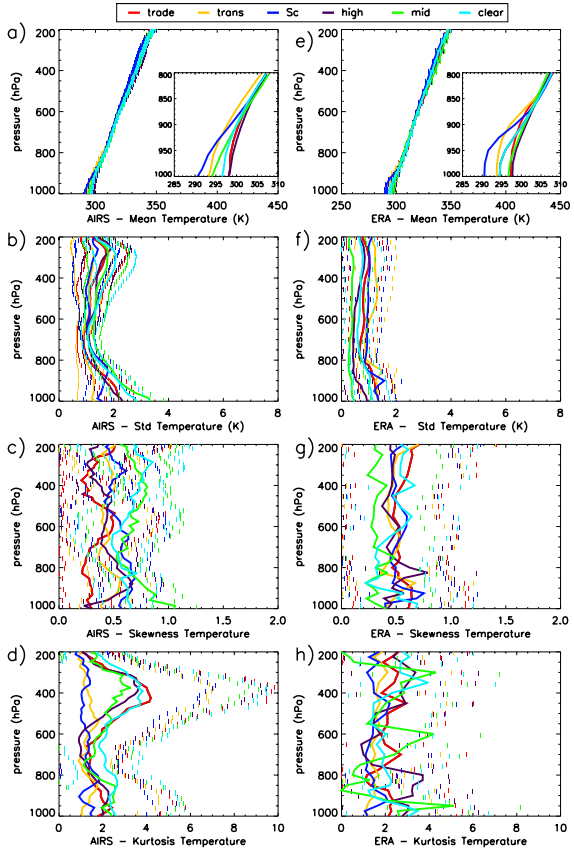

Fig. 5. The mean (panels **a** and **e**), standard deviation (panels **b** and **f**), skewness (panels **c** and **g**), and kurtosis (panels **d** and **h**) of the vertical profile of AIRS θ obtained from averages of the 217-day daily snapshots of AIRS/MODIS observations (left column), and ERA-Interim (right column). Dashed lines show the day-to-day variability of the moments.

ACPD
13, 24051–24085, 2013

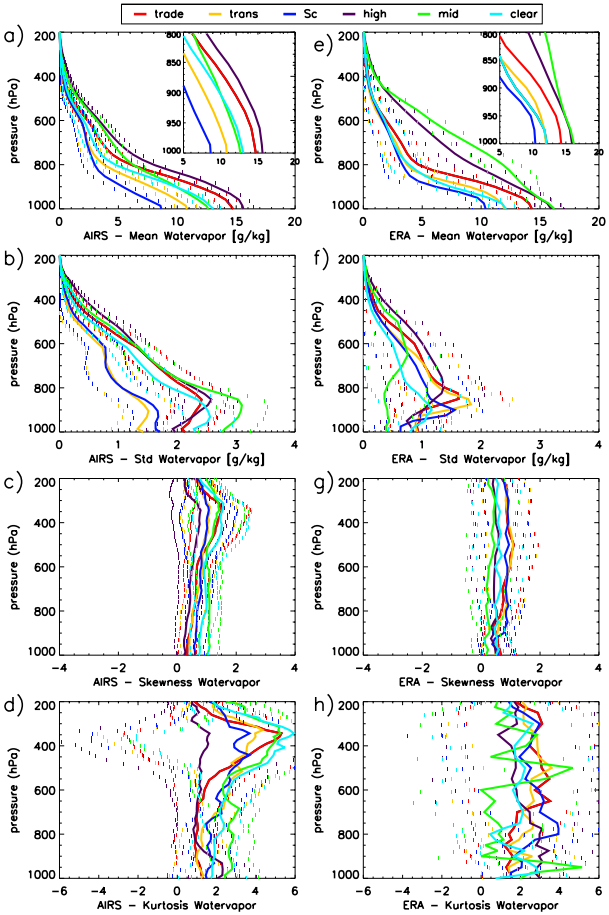

Fig. 6. The same as Fig. 5 except for the vertical profile of water vapor mixing ratio ($g\,kg^{-1}$).

ACPD
13, 24051–24085, 2013

Atmospheric parameters in a subtropical cloud regime transition

M. M. Schreier et al.